Structure of the deacetylase LpxC bound to the antibiotic CHIR-090: Time-dependent inhibition and specificity in ligand binding

Adam W. Barb, Ling Jiang[†], Christian R. H. Raetz, and Pei Zhou[‡]

Department of Biochemistry, Duke University Medical Center, Durham NC 27710

Communicated by Jane S. Richardson, Duke University Medical Center, Durham, NC, October 3, 2007 (received for review July 18, 2007)

The UDP-3-*O*-(*R*-3-hydroxyacyl)-*N*-acetylglucosamine deacetylase LpxC is an essential enzyme of lipid A biosynthesis in Gram-negative bacteria and a promising antibiotic target. CHIR-090, the most potent LpxC inhibitor discovered to date, displays two-step time-dependent inhibition and kills a wide range of Gram-negative pathogens as effectively as ciprofloxacin or tobramycin. In this study, we report the solution structure of the LpxC–CHIR-090 complex. CHIR-090 exploits conserved features of LpxC that are critical for catalysis, including the hydrophobic passage and essential active-site residues. CHIR-090 is adjacent to, but does not occupy, the UDP-binding pocket of LpxC, suggesting that a fragment-based approach may facilitate further optimization of LpxC inhibitors. Additionally, we identified key residues in the Insert II hydrophobic passage that modulate time-dependent inhibition and CHIR-090 resistance. CHIR-090 shares a similar, although previously unrecognized, chemical scaffold with other small-molecule antibiotics such as L-161,240 targeting LpxC, and provides a template for understanding the binding mode of these inhibitors. Consistent with this model, we provide evidence that L-161,240 also occupies the hydrophobic passage.

lipopolysaccharide | lipid A | *Aquifex aeolicus* | NMR

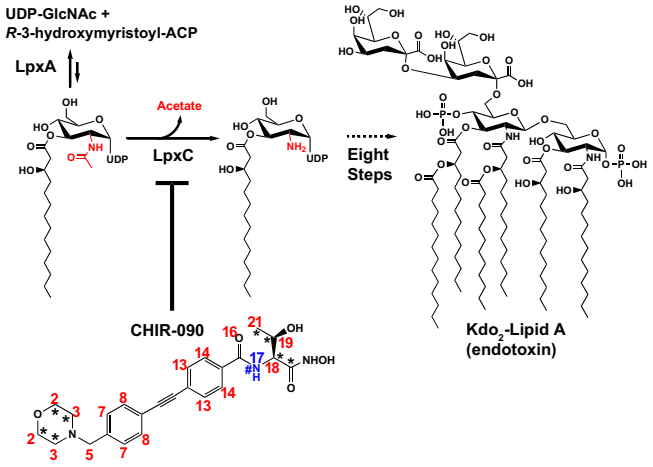

Fig. 1. The potent Gram-negative selective antibiotic CHIR-090 inhibits LpxC, which catalyzes the committed step of lipid A biosynthesis. The isotopically enriched CHIR-090 contained ^{13}C and ^{15}N at the positions indicated with * and #, respectively. The numbering of CHIR-090 is indicated.

The development of novel antibiotics is essential to combat emerging drug-resistant infections that threaten medicine's nearly 70-year predominance over bacterial pathogens. One of the most promising novel antibiotic targets of Gram-negative bacteria is the biosynthetic pathway of lipid A (endotoxin), typically a hexa-acylated disaccharide of glucosamine and the major lipid component of the outer leaflet of the outer membrane (1). Lipid A is the membrane anchor of lipopolysaccharide. It is an essential molecule that limits the diffusion of detergents and certain antibiotic compounds across the bacterial outer membrane (2).

Although lipid A biosynthesis begins with the thermodynamically unfavorable acylation of UDP-*N*-acetylglucosamine catalyzed by LpxA (Fig. 1) (3), the committed reaction of the pathway is the irreversible deacetylation of UDP-3-*O*-(*R*-3-hydroxyacyl)-*N*-acetylglucosamine catalyzed by the zinc-dependent enzyme LpxC (4). Inhibiting LpxC is lethal to *Escherichia coli*, and many LpxC inhibitors possess antibacterial properties, albeit with varying host ranges (5–7). CHIR-090 (Fig. 1), the most potent LpxC inhibitor described to date, controls the growth of *E. coli* and *Pseudomonas aeruginosa* in bacterial disk diffusion assays with an efficacy rivaling that of the commercial antibiotics ciprofloxacin or tobramycin (6). *In vitro*, CHIR-090 effectively inhibits the activities of a large number of LpxC orthologs at low nanomolar concentrations, including those from the pathogens *E. coli*, *Helicobacter pylori*, *Neisseria meningitidis*, and *P. aeruginosa*; however, CHIR-090 is a relatively weak inhibitor of LpxC from *Rhizobium leguminosarum* (8).

CHIR-090 is the first reported two-step, slow, tight-binding inhibitor of LpxC (6, 8). In contrast to a conventional inhibitor that forms only a rapidly dissociating enzyme:inhibitor (EI) complex, a two-step time-dependent inhibitor rapidly forms an encounter (EI) complex, followed by a slow isomerization to a terminal complex (EI*, Scheme 1) (9–11). Because a slow tight-binding inhibitor frequently resides on its target enzyme with a longer half-life than a conventional inhibitor, even when substrate accumulates, slow-binding inhibitors are highly desirable (12).

Extensive structural studies show that LpxC displays a novel "β-α-α-β sandwich" fold, formed by two domains with similar topologies (13–20). Each domain consists of a layer of two helices packing against a β-sheet containing mixed parallel and antiparallel strands, and the overall structure is characterized by the α-helices of each domain sandwiched between the β-sheets. Additionally, each domain contains a unique insert, with Insert I of Domain I consisting of a small β-sheet and Insert II of Domain II consisting of a unique β-α-β fold. LpxC binds the myristoyl chain of the hydroxamate-containing substrate-analog TU-514 within a hydrophobic passage that is largely formed by

Author contributions: A.W.B. and L.J. contributed equally to this work; A.W.B., L.J., C.R.H.R., and P.Z. designed research; A.W.B., L.J., and P.Z. performed research; A.W.B., L.J., and P.Z. analyzed data; and A.W.B., C.R.H.R., and P.Z. wrote the paper.

The authors declare no conflict of interest.

Data deposition: The atomic coordinates and NMR constraints have been deposited in the Protein Data Bank, www.pdb.org (PDB ID code 2JT2).

[†]Present address: State Key Laboratory of Magnetic Resonance and Atomic and Molecular Physics, Wuhan Institute of Physics and Mathematics, Chinese Academy of Sciences, Wuhan 430071, China.

[‡]To whom correspondence should be addressed. E-mail: peizhou@biochem.duke.edu.

This article contains supporting information online at www.pnas.org/cgi/content/full/0709412104/DC1.

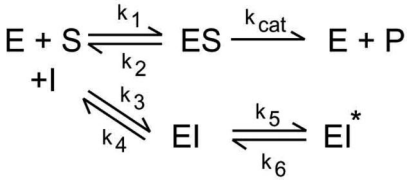

Scheme 1.

Insert II and a loop (β1-β2 loop) from Domain I (14, 15, 17). The lining of this passage mostly consists of conserved hydrophobic residues, providing high-affinity binding for the acyl chain of the substrate, and potentially, for the diverse range of potent LpxC inhibitors (15, 20).

Although previous structural studies of LpxC complexed with the substrate analog TU-514 or various weak-binding ligands have provided valuable insights into the mechanism of LpxC catalysis (14–17, 20, 21), the molecular details of high-affinity antibiotic recognition by LpxC remain unclear. Here we report the solution structure of LpxC bound to the most promising antibiotic lead compound CHIR-090 and identify key molecular features that confer binding specificity and affinity. Based on structural information, we further identify key residues in the hydrophobic passage of Insert II that are critical for the time-dependent inhibition of CHIR-090 and responsible for CHIR-090 resistance. Finally, we propose a consensus model for the recognition of structurally diverse inhibitors, which should facilitate the further improvement of antibiotics that target LpxC.

Results

Structure of the *Aquifex aeolicus* LpxC–CHIR-090 Complex. The LpxC–CHIR-090 complex was determined from 6,139 NOE, 643 dihedral angle, and 355 residual dipolar coupling constraints, and the binding interface was defined by 90 interfacial NOE constraints [supporting information (SI) Fig. 6 and SI Table 2]. The overall structure of LpxC in complex with CHIR-090 (Fig. 2) is very similar to other LpxC structures previously reported, with an average rmsd value of the backbone atoms of 0.54 Å, suggesting that binding of CHIR-090 does not induce large conformational changes of the hydrophobic passage or the overall structure of LpxC.

CHIR-090 exploits several conserved and essential features of LpxC to form a tight-binding complex (Fig. 3). These interactions can be divided into three distinct regions, as follows.

Threonyl-hydroxamate group. Like many other LpxC inhibitors, CHIR-090 contains a hydroxamate moiety coordinating the catalytic zinc ion (17). The binding of CHIR-090 is further strengthened through interactions with conserved hydrophilic and hydrophobic residues in the active site (Fig. 3). The amide proton (H17) of the CHIR-090 threonyl group is <2.0 Å away from the essential hydroxyl of T179 (22), with which it forms a hydrogen bond (Fig. 3). The T179A mutant of LpxC is less sensitive to CHIR-090 inhibition and, unlike wild-type *A. aeolicus* LpxC, appears to be reversibly inhibited by CHIR-090 (Fig. 3 *C* and *D*). The threonyl methyl group of CHIR-090 forms van der Waals (vdW) contacts with the aromatic ring of F180 (Fig. 3*B*), a residue that is likewise conserved and required for efficient catalysis (22). The threonyl hydroxyl oxygen atom of CHIR-090 is located within 3.5 Å of the absolutely conserved

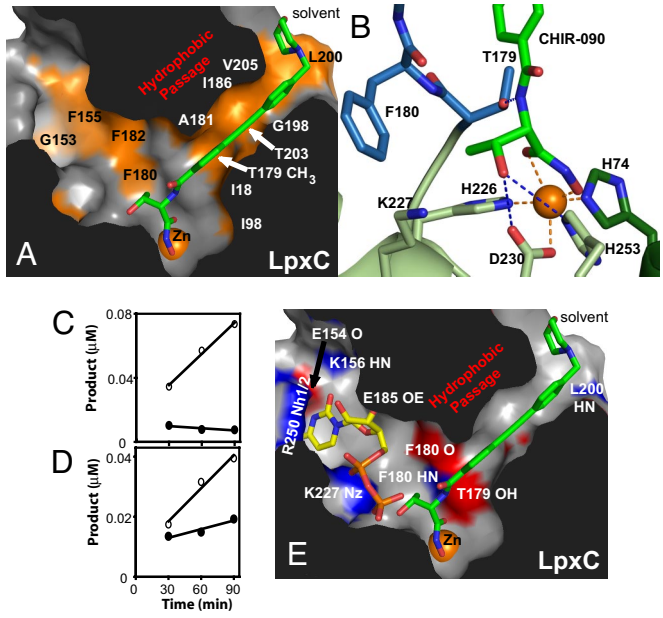

Fig. 3. Interface between CHIR-090 and LpxC. (*A*) CHIR-090 occupies the LpxC hydrophobic passage. Residues contributing to the hydrophobic surfaces are colored in orange and labeled. I189, which lies above the plane of the slice, is not shown. (*B*) Position of the CHIR-090 threonyl and hydroxamate groups in the active site. CHIR-090 is shown as a green stick model with oxygen and nitrogen atoms colored in red and blue, respectively, and the zinc ion is orange. LpxC residues are colored in accordance with the secondary structure elements as shown in Fig. 2*B*. (*C*) The activity of wild-type *A. aeolicus* LpxC with 0 nM (○) or 5 nM CHIR-090 (●). (*D*) The activity of the *A. aeolicus* LpxC T179A mutant with 0 nM CHIR-090 (○) or 5 nM CHIR-090 (●). (*E*) Potential hydrogen bond donors (blue) and acceptors (red) are highlighted on the surface of the UDP-binding pocket. CHIR-090 is shown as a green stick model, and UDP was modeled (from 2IER) and is shown as a yellow stick model with orange phosphorus atoms. In both cases oxygen and nitrogen atoms are colored in red and blue, respectively.

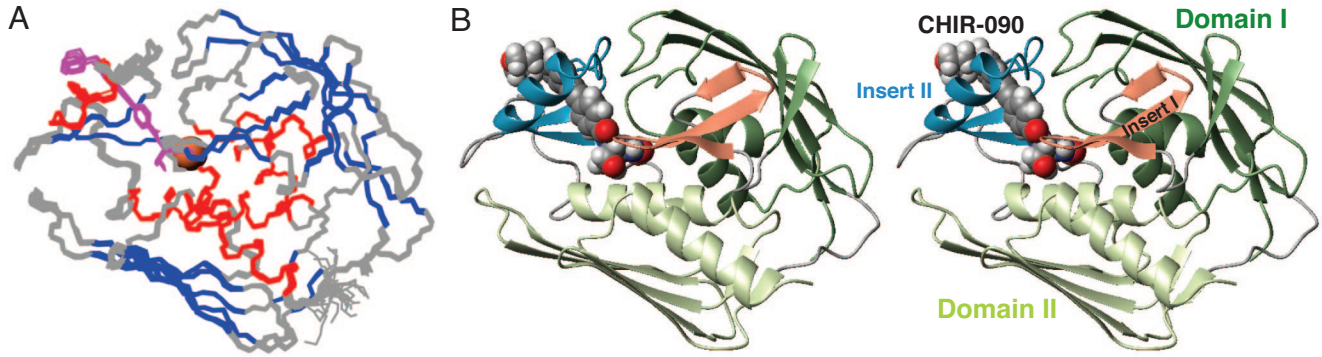

Fig. 2. Solution structure of the *A. aeolicus* LpxC–CHIR-090 complex. (*A*) NMR ensemble and (*B*) ribbon diagram (stereoview) of the complex of LpxC and CHIR-090. The catalytic zinc ion is shown as an orange sphere. This figure was prepared by using MolMol (35).

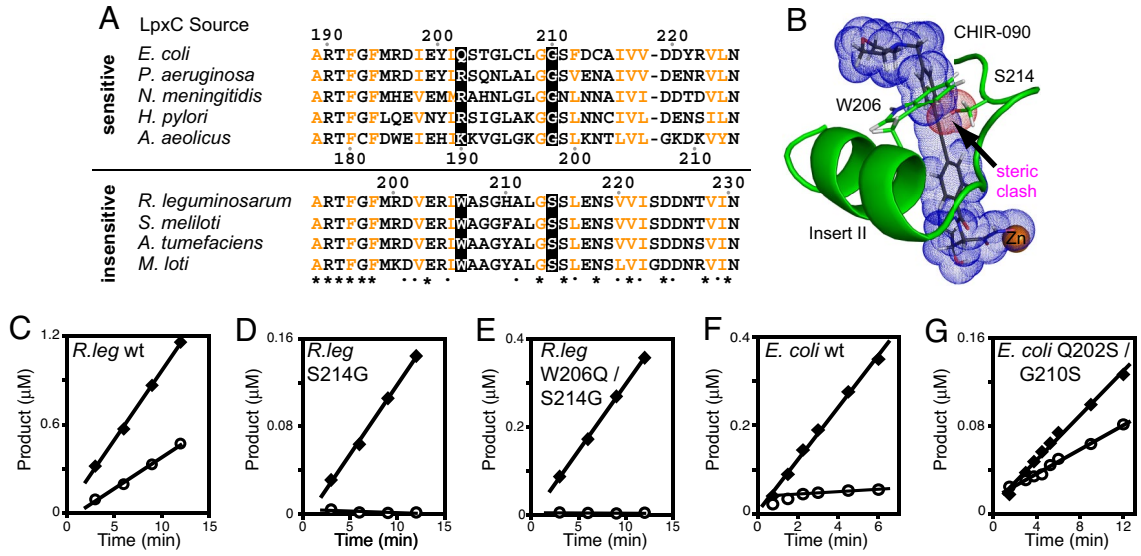

Fig. 4. LpxC Insert II residues in the hydrophobic passage are critical for CHIR-090 resistance and time-dependent inhibition. (*A*) Sequence alignment of LpxC orthologs from CHIR-090-sensitive and -insensitive bacteria. Conserved hydrophobic residues are colored in orange. The amino acids tested in this work are highlighted with a black background. Residue numbers for *A. aeolicus*, *E. coli*, and *R. leguminosarum* LpxC are included. (*B*) Homology model of *R. leguminosarum* LpxC Insert II with CHIR-090. CHIR-090 and the Ser and Trp side chains are shown as stick models. The vdW surfaces of CHIR-090 and the Ser 214 hydroxyl group are shown as blue and red dots, respectively. (*C–G*) Sensitivity of mutant LpxC enzymes to CHIR-090. The wild-type *R. leguminosarum* enzyme (*C*) and the mutant enzymes S214G (*D*) and W206Q/S214G (*E*) were assayed with 0 μM CHIR-090 (◆) or 0.5 μM CHIR-090 (○). The wild-type *E. coli* enzyme (*F*) and the mutant enzyme Q202W/G210S (*G*) were assayed with 0 nM CHIR-090 (◆) or 4 nM CHIR-090 (○). The linear portion of the reaction velocity is depicted with a line.

residues H253 (Nε2) and D230 (Oδ2). Both the D230 carboxylate and the positively charged H253 imidazole group (15) are well positioned to form hydrogen bonds with CHIR-090. Although the side-chain ε-amino group of K227 (which is part of the unique HKΦΦD motif of LpxC) is not well defined in the NMR-derived (NMR) ensemble, the distance from these amine protons to the CHIR-090 threonyl hydroxyl oxygen atom, varies from 2.8 to 5.7 Å. K227 is therefore another potential hydrogen-bonding partner for the CHIR-090 hydroxyl group. The carbonyl oxygen (O16) of CHIR-090 does not appear to be specifically coordinated by LpxC.

The biphenyl acetylene unit. The biphenyl acetylene moiety of CHIR-090 inserts into the LpxC hydrophobic passage near the active site and protrudes from the opposite end of this passage (Fig. 3*A*), similar to TU-514 and fatty acids (14, 15, 20). Extensive interfacial NOEs are observed between CHIR-090 and residues within the passage, including I18, I186, I189, G198, L200, T203, and V205, many of which are conserved as either a methyl-containing and/or hydrophobic residue (Fig. 3 and SI Fig. 6). Within the hydrophobic passage, the CHIR-090 aromatic rings are not coplanar but are offset by a −25° dihedral angle. Analysis of space-filling models of CHIR-090 and LpxC reveals highly complementary surfaces.

The morpholine unit. The distal end of the LpxC hydrophobic passage opens at the surface of the protein, forming part of a shallow hydrophobic pocket that is offset to one side of the hydrophobic passage. The morpholine ring of CHIR-090 is positioned at an ≈110° angle relative to the long axis of the biphenyl acetylene moiety and fits into this shallow hydrophobic pocket. In most models, the morpholine ring adopts a boat conformation and lies flat, with one face against the LpxC surface and the other face exposed to solvent. Minor conformations, such as chair or twisted chair, are also present in the NMR ensemble. The presence of strong NOEs between the morpholine ring and methyl groups of I186, L200 and V205, as well as Y212, indicates that the morpholine ring is bound through hydrophobic interactions (Fig. 3). The morpholine ring does not appear to be coordinated by hydrogen bonding, despite the potential hydrogen bond accepting O and N atoms.

Molecular Determinants of CHIR-090 Resistance. Most LpxC enzymes, including those from *E. coli*, *P. aeruginosa*, *N. meningitidis*, *H. pylori*, and *A. aeolicus*, are inhibited by nanomolar concentrations of CHIR-090 in a time-dependent manner (6, 8). In contrast, four Gram-negative bacteria from the Rhizobeaceae family, *R. leguminosarum*, *Sinorhizobium meliloti*, *Mesorhizobium*

Table 1. Inhibition of wild-type and mutant LpxC proteins

Source	CHIR-090, K_i, nM	CHIR-090, K_i^*, nM	L-161,240, K_i, μM	BB-78485, K_i, μM
E. coli LpxC				
Wild type	4.0 ± 1.0[†]	0.5 ± 0.1[†]	0.053 ± 0.016	0.069 ± 0.015
Q202W/G210S	5.0 ± 1.7	n.a.	0.34 ± 0.07	0.086 ± 0.028
R. leguminosarum LpxC				
Wild type	340 ± 60[†]	n.a.	380 ± 70	5.8 ± 0.9
S214G	3.5 ± 2.3	n.a.	ND	ND
W206Q/S214G	3.0 ± 1.4	n.a.	110 ± 60	0.70 ± 0.40

n.a., not applicable; ND, not determined.
[†]Ref. 8.

loti, and *Agrobacterium tumefaciens*, are insensitive to CHIR-090, as judged by disk-diffusion assays (8). LpxC from *R. leguminosarum* (43% amino acid sequence identity to *E. coli* LpxC) is orders of magnitude less sensitive to CHIR-090 (680-fold) than *E. coli* LpxC and is not inhibited by CHIR-090 in a time-dependent manner.

Any amino acids responsible for this striking decrease in affinity are likely located within the inhibitor-binding site. By aligning the sequences of five CHIR-090-sensitive and four -insensitive LpxCs, we identified two residues within Insert II surrounding the hydrophobic passage that are significantly different between these two categories (Fig. 4*A*). The most compelling difference is the presence of a Ser residue in the CHIR-090-insensitive proteins (S214 of *R. leguminosarum* LpxC), which is Gly in the CHIR-090-sensitive proteins (G210 of *E. coli* and G198 of *A. aeolicus* LpxC). Additionally, a Trp residue is found in the CHIR-090-insensitive proteins (W206 of *R. leguminosarum* LpxC), whereas variable residues with smaller side chains (Gln, Lys, or Arg) predominate in the CHIR-090-sensitive proteins (Q202 of *E. coli* and K190 of *A. aeolicus* LpxC).

Homology modeling of *R. leguminosarum* LpxC using XLOOK (23) suggests that the side chain of S214 of *R. leguminosarum* LpxC would partially occlude the hydrophobic passage and introduce a hydrophilic moiety not present in *A. aeolicus* LpxC (Fig. 4*B*). Assuming that CHIR-090 binds within the *R. leguminosarum* LpxC passage in a manner that is similar to the mode observed for *A. aeolicus* LpxC, the hydroxyl group of S214 (in every possible side-chain rotamer) would severely clash with the inhibitor. Unlike S214, W206 of *R. leguminosarum* LpxC would not clash with CHIR-090 (Fig. 4*B*); however, the presence of a bulky Trp residue would severely restrict the conformational space of Insert II and narrow the exit of the hydrophobic passage.

To investigate the role of these two residues in LpxC inhibition, the appropriate single and double mutants of *E. coli* and *R. leguminosarum* LpxC were overexpressed, purified, and analyzed for catalytic activity. *E. coli* LpxC was chosen as a representative CHIR-090 sensitive enzyme, considering the variety and potency of available *E. coli* LpxC inhibitors (5, 7) and the fact that L-161,240 and BB-78485 do not inhibit *A. aeolicus* LpxC.

All mutant enzymes displayed typical Michaelis–Menten kinetics (SI Table 3). The sensitivity of each enzyme to CHIR-090 inhibition was evaluated with an enzyme activity assay in the presence of CHIR-090. The activity of *R. leguminosarum* LpxC was reduced by ≈50% in the presence of 0.5 μM CHIR-090 (Fig. 4*C*); however, the activity of both the S214G and W206Q/S214G mutant proteins was completely inhibited under the same conditions (Fig. 4 *D* and *E*). No evidence of time-dependent inhibition was observed in assays with either the wild-type or mutant *R. leguminosarum* LpxCs (data not shown). IC_{50} experiments determined that *R. leguminosarum* LpxC S214G is 100-fold more sensitive to CHIR-090 than the wild-type enzyme, with a K_i of 3.5 ± 2.3 nM; a similar result was observed for the W206Q/S214G mutant with a K_i of 3.0 ± 1.4 nM (Table 1).

The opposite trend was seen for the mutants of *E. coli* LpxC. The activities of wild-type and single mutants of *E. coli* LpxC were inhibited >75% by 4 nM CHIR-090 (wild type in Fig. 4*F*; single mutant data not shown), but the LpxC double-mutant Q202W/G210S was significantly less sensitive to CHIR-090 (Fig. 4*G*). Importantly, CHIR-090 was no longer a time-dependent inhibitor of the *E. coli* LpxC double mutant, as judged by an analysis of reaction progress curves (Fig. 4*G*) and a preincubation/dilution experiment (8) (data not shown), suggesting that the slow-binding complex was not formed. Therefore, we designate the terminal *E. coli* LpxC Q202W/G210S–CHIR-090 complex "EI" with an equilibrium dissociation constant K_i. The K_i (5.0 nM) for the double mutant Q202W/G210S of *E. coli* LpxC is 10-fold greater than the equilibrium dissociation constant (K_i^* of 0.5 nM) of the slowly forming wild-type *E. coli* LpxC–CHIR-090 EI* complex (Table 1), but it is nearly identical to the K_i (4.0 nM) of the wild-type LpxC–CHIR-090 encounter complex (EI) (8).

A Consensus-Binding Mode for Potent LpxC Inhibitors. Comparison of CHIR-090 with two other potent LpxC inhibitors, L-161,240 (7) and BB-78485 (5), reveals striking, although previously unrecognized, similarities (Fig. 5*A*). These compounds share a hydroxamate moiety, which is necessary to coordinate the catalytic zinc ion, and, continuing away from the hydroxamate, a chiral carbon. Different moieties are attached to the chiral carbon at either the R_1 or R_1' positions. L-161,240 and BB-78485 have bulky substitutions at R_1 and a proton at R_1', and these compounds are thus *R* enantiomers (Fig. 5*A*). CHIR-090, which is an *S* enantiomer containing an L-threonyl moiety, has a proton at R_1 and the threonine side chain at R_1'.

Adjacent to the chiral carbon, each compound contains a nitrogen atom, which may be an amide (CHIR-090), a sulfonamide (BB-78485), or nitrogen in an oxazoline ring (L-161,240). The CHIR-090 amide proton forms a hydrogen bond with the T179 hydroxyl group, and the coordination of BB-78485 is likely

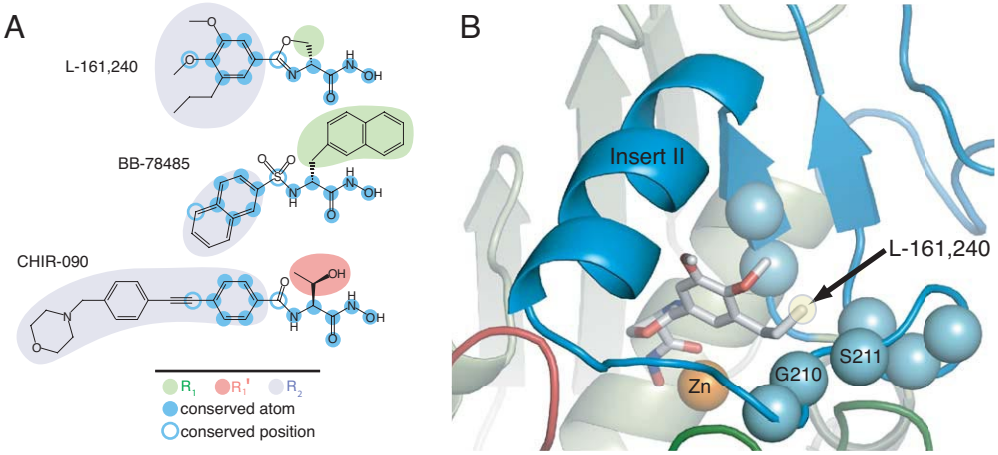

Fig. 5. Common features of structurally diverse LpxC inhibitors. (*A*) Comparison of L-161,240, BB-78485, and CHIR-090 revealed conserved atoms and positions (R_1, R_1', and R_2). (*B*) Model of L-161,240 bound to *E. coli* LpxC based on a saturation transfer difference (STD) experiment. Residues with amide resonances affected by saturating the terminal methyl proton resonance of the L-161,240 propyl group (indicated by a transparent yellow halo) are shown as spheres on a homology model. L-161,240 is shown as a white stick model.

similar. Although L-161,240 does not have a hydrogen-bond donor at this position, the nitrogen in the oxazoline ring could accept a hydrogen bond from the T179 hydroxyl or the nearby F180 amide.

The next similar position is either a sulfur or carbon atom, followed by the R_2 substitution, which includes an aromatic ring in each of these compounds (Fig. 5*A*). According to our binding model, R_2 substituents are positioned to insert into the hydrophobic passage of LpxC. This analysis predicts that the substituted phenyl group of L-161,240 and the naphthalene group adjacent to the sulfonamide of BB-78485 likewise occupy the LpxC hydrophobic passage.

Mutations in the LpxC Insert II region, previously shown to alter the sensitivity of LpxC to CHIR-090 inhibition, similarly affected the binding affinity of L-161,240 and BB-78485 (Table 1), indicating that Insert II is a critical component of LpxC binding to L-161,240 and BB-78485. However, the effect of the mutations is much less pronounced, presumably because the shorter R_2 groups of L-161,240 and BB-78485 do not penetrate as deep as CHIR-090 into the hydrophobic passage.

Supporting the activity measurements, selective saturation of the terminal methyl group of the propyl substituent of L-161,240 bound to *E. coli* LpxC resulted in attenuation of amide resonances from F192, G193, G209, G210, S211, D213, C214, and A215, suggesting that these residues are located in close proximity to the L-161,240 propyl terminus (Fig. 5*B*). Because these residues are located within Insert II, this magnetic resonance-based measurement provides experimental evidence to position the L-161,240 propyl group within the hydrophobic passage of *E. coli* LpxC.

Discussion

CHIR-090 is the most potent LpxC inhibitor discovered to date, displaying the broadest range of Gram-negative antibiotic activity (6, 8). The high affinity of CHIR-090 for LpxC is likely due to three factors in addition to its chelation of the active site zinc ion: its shape, rigidity, and hydrophobicity.

The surface of CHIR-090 is highly complementary to the "L"-shaped hydrophobic passage of LpxC. The biphenyl acetylene moiety of CHIR-090 is similar in size and shape to the acyl chain of the substrate analog TU-514 and to the various fatty acids that can occupy the passage (14, 17, 20). The rigid structure of CHIR-090 likely contributes to the high-affinity interaction, because the loss of conformational entropy upon binding is significantly reduced compared with the flexible acyl chain-containing compounds, like TU-514. Most of the protein–CHIR-090 interface is characterized by hydrophobic interactions within the Insert II passage. Because the hydrophobic nature of this passage is strictly conserved among diverse LpxC orthologs, disrupting these CHIR-090–LpxC interactions is expected to impact the binding of the natural substrate negatively, thereby reducing catalytic activity.

LpxC active-site residues that interact with CHIR-090 are also highly conserved and required for efficient catalysis (21, 22, 24). CHIR-090 specifically coordinates the conserved side-chain hydroxyl of T179, which is occasionally substituted with Ser in some orthologs. H253 and D230 are absolutely conserved across all known LpxC orthologs, and F180 is infrequently substituted with Tyr.

CHIR-090's exploitation of highly conserved LpxC features may partially explain the extremely low incidence of spontaneous resistance compared with L-161,240 and BB-78485 (5, 8).

The tandem Q202W and G210S mutations of *E. coli* LpxC, containing *R. leguminosarum* LpxC residues at the corresponding positions, abolished the slow tight-binding kinetics of CHIR-090 seen with the wild-type enzyme. Although the hydrophobic passage, which largely consists of Insert II and the $\beta1$-$\beta2$ loop (Fig. 4), appears rigid in our structure, this fixed architecture does not permit the binding of CHIR-090 without major conformational changes. Evidence for conformational exchange of Insert II among multiple states has been reported (14), suggesting that binding and release of the substrate may be accompanied by alternation between closed and open conformations of the enzyme during catalysis. Such an open conformation may also be required to permit insertion of CHIR-090 into the hydrophobic passage.

Our data further suggest that Insert II is critical for time-dependent inhibition. The structural basis for time-dependent inhibition likely originates from the rigidity of CHIR-090, which may allow for the rapid formation of an encounter (EI) complex (Scheme 1), involving zinc coordination by CHIR-090, a loose interaction between CHIR-090 and the enzyme, and a partially structured hydrophobic passage. The subsequent slow step of CHIR-090 binding to LpxC may require the reorganization of Insert II around the rigid CHIR-090 molecule, forming the tight-binding complex. Supporting this interpretation, the affinity of the double-mutant *E. coli* LpxC toward CHIR-090 (K_i = 5.0 ± 1.7 nM) is nearly identical to that of the rapidly forming encounter complex of the wild-type enzyme (K_i = 4.0 ± 1.0 nM). This finding suggests that the Q202W and G210S mutations disrupt the final complex but have a negligible effect on the formation of the initial encounter complex. Time-dependent behavior has not been observed with substrate-analog inhibitor (TU-514) binding, despite the fact that the acyl chain of TU-514 occupies the same hydrophobic passage as the biphenyl acetylene moiety of CHIR-090. The inherent flexibility of the TU-514 acyl chain may permit additional conformational adjustments during the reorganization of Insert II, which are not accessible with CHIR-090. Taken together, our data suggest that both the conformational dynamics of Insert II and the rigidity of CHIR-090 are critical components of time-dependent inhibition.

This structure of the LpxC-CHIR090 complex suggests two solutions to improving the potency of CHIR-090. First, the CHIR-090 threonyl group is located adjacent to, but does not occupy, the UDP-binding pocket, which is common to all LpxC orthologs (Fig. 3*E*) (16). Analysis of the UDP pocket reveals conserved hydrogen bond donors and acceptors, as well as hydrophobic surfaces that might be readily accessed by a CHIR-090 analog. Thus, expanding the binding area of CHIR-090 to the UDP site may be an effective means to improve potency. Second, the CHIR-090 morpholine unit could be improved to enhance inhibitor binding to LpxC by reducing the conformational heterogeneity of this relatively flexible moiety.

In summary, our data suggest that the long, rigid nature of CHIR-090 and the interaction with the LpxC Insert II region of the hydrophobic passage are critical to potency and time dependency. These observations suggest a consensus-binding model for other potent LpxC inhibitors. Future structural studies of other LpxC orthologs and unliganded *A. aeolicus* LpxC will provide additional insights into the mechanism and design of broad-spectrum Gram-negative antibiotics targeting the lipid A pathway.

Methods

Materials and Reagents. Unlabeled and isotopically enriched CHIR-090 and the *R*/*S* mixture of BB-78485 (of which only *R* is an inhibitor) were prepared at the Duke University Small Molecule Synthesis Facility according to published procedures (5, 25). The *R* enantiomer of L-161,240 was synthesized as described (26). Stable isotopes were purchased from Cambridge Isotope Laboratory. Pf1 filamentous phage was purchased from ASLA.

Sample Preparation. A plasmid encoding wild-type *A. aeolicus* LpxC lacking the eight C-terminal amino acids and containing a C181A mutation was prepared by using the QuikChange site-directed mutagenesis kit (Stratagene) from cloned *A. aeolicus* LpxC (26). LpxC protein was expressed and purified as described (14). Con-

centrated LpxC was exchanged into 25 mM sodium phosphate (pH 7.0) and 100 mM KCl. CHIR-090 was dissolved in DMSO and added to the protein solution such that the final DMSO concentration was 5% (vol/vol). The LpxC–CHIR-090 complex was incubated at 45°C for 4 days to obtain a homogenous sample. Excess CHIR-090 (1.2- to 1.5-fold) was used to prepare the sample to ensure formation of the LpxC–CHIR-090 complex. DMSO and unbound CHIR-090 were removed using a Sephacryl S-200 HR column (GE Healthcare). NMR samples contained 0.8–1.0 mM LpxC–CHIR-090 complex.

NMR Spectroscopy and Structure Calculation. All NMR experiments were performed at 45°C on Varian INOVA 600 and 800 MHz spectrometers equipped with cold probes. Data were processed using NMRPIPE (27) and analyzed with XEASY/CARA (28). Details about the specific NMR-based experiments may be found in *SI Text*.

Initial structures were calculated using the combined input of automated analysis implemented in CYANA 2.1 (29) and manual assignment. The structures were then refined against residual dipolar couplings using XPLOR-NIH (30). Zinc coordination was restrained with two hydroxamate atoms (O22 and O24 of CHIR-090) and three residues of LpxC (H74, H226, and D230) based on recent crystallographic evidence (17), but the orientation of the hydroxamate group was allowed to float in the calculation. Twenty-five models of the LpxC–CHIR-090 complex with no NOE violations >0.5 Å and no dihedral angle violations >5° were calculated and evaluated by MOLPROBITY (31). Structure figures were generated by using PyMOL (DeLano Scientific), unless otherwise noted.

Kinetic Analysis of Mutant LpxC Activities. Plasmids encoding mutant *E. coli* LpxC and *R. leguminosarum* LpxC (8) were generated by using the QuikChange kit (Stratagene) from wild-type *E. coli* LpxC and *R. leguminosarum* LpxC and verified by DNA sequencing (Duke University DNA Analysis Facility). Wild-type and mutant proteins were expressed, purified, and assayed as described (8). LpxC activity assays contained 5 μM UDP-3-*O*-(*R*-3-hydroxymyristoyl)-*N*-acetylglucosamine, unless otherwise noted. K_M and k_{cat} values were determined by using data sets containing multiple independent experiments. The K_i values were determined by varying inhibitor concentration while maintaining 10% DMSO in the assay. An IC_{50} curve was fit to the fractional activity (v_i/v_o) data, and a K_i value was determined by using the Cheng–Prusoff relationship (32). Standard IC_{50} experiments were performed with those proteins not inhibited by CHIR-090 in a time-dependent manner (8, 33). Because BB-78485 (*R*/*S*) used in our assays is a racemic mixture, the reported K_i values refer only to the active (*R*) enantiomer with the assumption of an *R*:*S* ratio of 1:1.

NMR of *E. coli* LpxC. Using a uniformly ^{2}H- and ^{15}N-labeled protein, a saturation-transfer difference (STD) ^{1}H-^{15}N HSQC experiment (34) was used to identify *E. coli* LpxC amide protons close to the propyl-methyl group of L-161,240 by selectively saturating the compound signal. The identities of the saturation-transfer-attenuated amide resonances were assigned from triple-resonance experiments of the *E. coli* LpxC – L-161,240 complex (A.W.B. and P.Z., unpublished work).

We thank Drs. Johannes Rudolph, David Six, and Brian Coggins for helpful discussions. This research was supported by National Institutes of Health Grants AI-055588 (to P.Z.) and GM-51310 (to C.R.H.R.) and by the Whitehead Foundation (P.Z.). A.W.B. was supported by Cell and Molecular Biology Training Grant GM-07184 (to Duke University).

1. Raetz CRH, Whitfield C (2002) *Annu Rev Biochem* 71:635–700.
2. Raetz CRH (1996) in *Escherichia coli and Salmonella: Cellular and Molecular Biology* (ASM Press, Washington, DC), pp 1035–1063.
3. Anderson MS, Bulawa CE, Raetz CRH (1985) *J Biol Chem* 260:15536–15541.
4. Anderson MS, Robertson AD, Macher I, Raetz CRH (1988) *Biochemistry* 27:1908–1917.
5. Clements JM, Coignard F, Johnson I, Chandler S, Palan S, Waller A, Wijkmans J, Hunter MG (2002) *Antimicrob Agents Chemother* 46:1793–1799.
6. McClerren AL, Endsley S, Bowman JL, Andersen NH, Guan Z, Rudolph J, Raetz CRH (2005) *Biochemistry* 44:16574–16583.
7. Onishi HR, Pelak BA, Gerckens LS, Silver LL, Kahan FM, Chen MH, Patchett AA, Galloway SM, Hyland SA, Anderson MS, Raetz CRH (1996) *Science* 274:980–982.
8. Barb AW, McClerren AL, Karnam S, Reynolds CM, Zhou P, Raetz CRH (2007) *Biochemistry* 46:3793–3802.
9. Morrison JF (1969) *Biochim Biophys Acta* 185:269–286.
10. Morrison JF, Walsh CT (1988) *Adv Enzymol Relat Areas Mol Biol* 61:201–301.
11. Williams JW, Morrison JF (1979) *Methods Enzymol* 63:437–467.
12. Swinney DC (2004) *Nat Rev Drug Discov* 3:801–808.
13. Buetow L, Dawson A, Hunter WN (2006) *Acta Crystallogr* F62:1082–1086.
14. Coggins BE, Li X, McClerren AL, Hindsgaul O, Raetz CRH, Zhou P (2003) *Nat Struct Biol* 10:645–651.
15. Coggins BE, McClerren AL, Jiang L, Li X, Rudolph J, Hindsgaul O, Raetz CRH, Zhou P (2005) *Biochemistry* 44:1114–1126.
16. Gennadios HA, Christianson DW (2006) *Biochemistry* 45:15216–15223.
17. Gennadios HA, Whittington DA, Li X, Fierke CA, Christianson DW (2006) *Biochemistry* 45:7940–7948.
18. Hernick M, Fierke CA (2005) *Arch Biochem Biophys* 433:71–84.
19. McClure CP, Rusche KM, Peariso K, Jackman JE, Fierke CA, Penner-Hahn JE (2003) *J Inorg Biochem* 94:78–85.
20. Whittington DA, Rusche KM, Shin H, Fierke CA, Christianson DW (2003) *Proc Natl Acad Sci USA* 100:8146–8150.
21. Hernick M, Gennadios HA, Whittington DA, Rusche KM, Christianson DW, Fierke CA (2005) *J Biol Chem* 280:16969–16978.
22. Hernick M, Fierke CA (2006) *Biochemistry* 45:15240–15248.
23. Lee C (1999) *LOOK: A Software System for Integrated Macromolecular Sequence-Structure Analysis and Modeling* (Molecular Applications Group, Palo Alto, CA).
24. McClerren AL, Zhou P, Guan Z, Raetz CRH, Rudolph J (2005) *Biochemistry* 44:1106–1113.
25. Andersen NH, Bowman J, Erwin AL, Harwood EA, Kline T, Mdluli K, Pfister KB, Shawar R, Wagman A, Yabannavar A (2004) World Intellectual Property Organization WO Patent 2004/062601 A2.
26. Jackman JE, Fierke CA, Tumey LN, Pirrung M, Uchiyama T, Tahir SH, Hindsgaul O, Raetz CRH (2000) *J Biol Chem* 275:11002–11009.
27. Delaglio F, Grzesiek S, Vuister GW, Zhu G, Pfeifer J, Bax A (1995) *J Biomol NMR* 6:277–293.
28. Bartels C, Xia TH, Billeter M, Güntert P, Wüthrich K (1995) *J Biomol NMR* 5:1–10.
29. Güntert P, Mumenthaler C, Wüthrich K (1997) *J Mol Biol* 273:283–298.
30. Brunger AT, Adams PD, Clore GM, DeLano WL, Gros P, Grosse-Kunstleve RW, Jiang JS, Kuszewski J, Nilges M, Pannu NS, *et al.* (1998) *Acta Crystallogr D* 54:905–921.
31. Davis IW, Leaver-Fay A, Chen VB, Block JN, Kapral GJ, Wang X, Murray LW, Arendall BW, Richardson JS, Richardson DC (2007) *Nucleic Acids Res* 35:W375–W383.
32. Cheng Y, Prusoff WH (1973) *Biochem Pharmacol* 22:3099–3108.
33. Copeland RA (2005) *Evaluation of Enzyme Inhibitors in Drug Discovery: A Guide for Medicinal Chemists and Pharmacologists* (Wiley Interscience, Hoboken, NJ).
34. Mayer M, Meyer B (1999) *Angew Chem Int Ed* 38:1784–1789.
35. Koradi R, Billeter M, Wüthrich K (1996) *J Mol Graphics* 14:51–55: 29–32.

Corrections

BIOCHEMISTRY. For the article "Structure of the deacetylase LpxC bound to the antibiotic CHIR-090: Time-dependent inhibition and specificity in ligand binding," by Adam W. Barb, Ling Jiang, Christian R. H. Raetz, and Pei Zhou, which appeared in issue 47, November 20, 2007, of *Proc Natl Acad Sci USA* (104:18433–18438; first published November 19, 2007; 10.1073/pnas.0709412104, the authors note that Fig. 4 appeared incorrectly. In Fig. 4*A*, in the *E. coli* LpxC sequence, the residues "QS**T**GLCLGG" should instead appear as "QS**R**GLCLGG." Additionally, Fig. 4*G* was mislabeled. These errors do not affect the conclusions of the article. The corrected figure and its legend appear below.

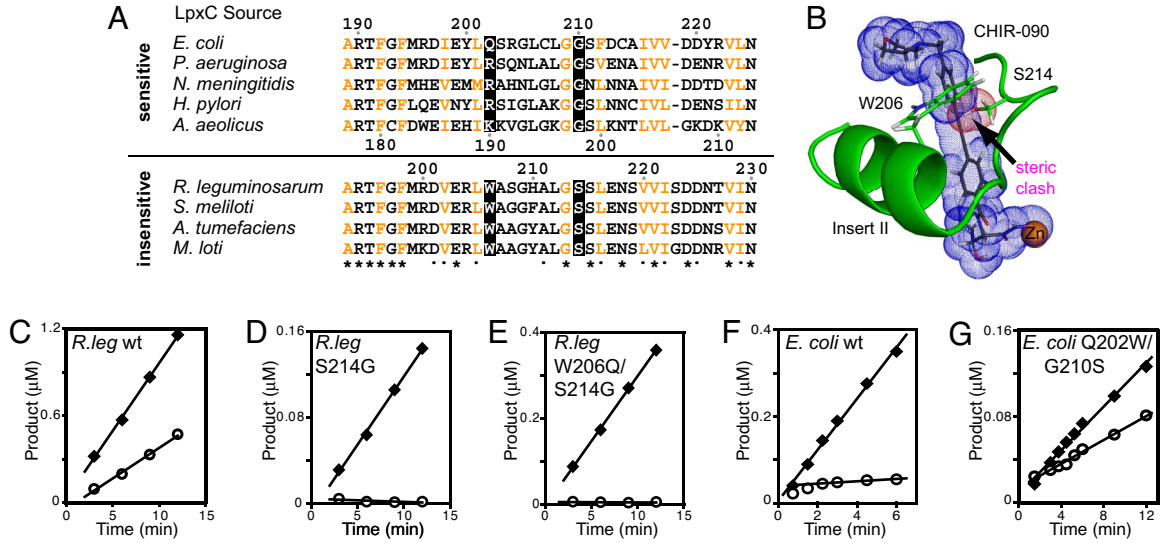

Fig. 4. LpxC Insert II residues in the hydrophobic passage are critical for CHIR-090 resistance and time-dependent inhibition. (*A*) Sequence alignment of LpxC orthologs from CHIR-090-sensitive and -insensitive bacteria. Conserved hydrophobic residues are colored in orange. The amino acids tested in this work are highlighted with a black background. Residue numbers for *A. aeolicus*, *E. coli*, and *R. leguminosarum* LpxC are included. (*B*) Homology model of *R. leguminosarum* LpxC Insert II with CHIR-090. CHIR-090 and the Ser and Trp side chains are shown as stick models. The vdW surfaces of CHIR-090 and the Ser 214 hydroxyl group are shown as blue and red dots, respectively. (*C–G*) Sensitivity of mutant LpxC enzymes to CHIR-090. The wild-type *R. leguminosarum* enzyme (*C*) and the mutant enzymes S214G (*D*) and W206Q/S214G (*E*) were assayed with 0 μM CHIR-090 (◆) or 0.5 μM CHIR-090 (○). The wild-type *E. coli* enzyme (*F*) and the mutant enzyme Q202W/G210S (*G*) were assayed with 0 nM CHIR-090 (◆) or 4 nM CHIR-090 (○). The linear portion of the reaction velocity is depicted with a line.

www.pnas.org/cgi/doi/10.1073/pnas.0711065105

COMMENTARY. For the article "Calcium channels in higher-level brain function," by Edward G. Jones, which appeared in issue 46, November 13, 2007, of *Proc Natl Acad Sci USA* (104:17903–17904; first published November 7, 2007; 10.1073/pnas.0709509104), the author notes that, due to a printer's error, ref. 1 appeared incorrectly in part. The author name **Hee-Sup S** should have appeared as **Shin H-S**. The corrected ref. 1 should read: "Llinás RR, Choi S, Urbano FJ, Shin H-S (2007) *Proc Natl Acad Sci USA* 104:17819–17824."

www.pnas.org/cgi/doi/10.1073/pnas.0711056105